

Electron Rutherford back-scattering case study: oxidation and ion implantation of aluminium foil

M. R. Went* and M. Vos

Atomic and Molecular Physics Laboratories, Research School of Physical Sciences and Engineering, Australian National University, Canberra, ACT 0200, Australia

Received 12 June 2007; Revised 19 August 2007; Accepted 3 September 2007

Electron Rutherford back scattering (ERBS) is a new spectroscopy for determining the composition of surfaces. In this work the surface sensitivity of ERBS was investigated by changing the entrance and exit angle of the electron beam while keeping the scattering angle constant. It was found that in this way the surface sensitivity of the technique can be varied considerably. We use aluminium as a test case for ERBS, as it is well studied. The technique has been used to investigate the oxide film of aluminium foil as manufactured and the native oxide (Al_2O_3) film formed on a clean aluminium surface exposed to air. We have also used ERBS to investigate the presence of Xe, implanted during the sputter cleaning process, at a variety of depths within an aluminium matrix. Copyright © 2007 John Wiley & Sons, Ltd.

KEYWORDS: aluminium; aluminium oxide; electron Rutherford back scattering; Rutherford back scattering

INTRODUCTION

Electron Rutherford back scattering (ERBS) is a relatively new surface analysis technique.^{1–4} Analogous to (ion) Rutherford back scattering (RBS), it relies on the elastic scattering of particles from the surface and near-surface region at high-momentum transfer. However, in ERBS the scattered particles are electrons rather than ions. Electrons, which scatter elastically from materials, are often naïvely thought to have the same incident and exit energy because of the relatively large mass ratio between the target and projectile. In reality, only the total kinetic energy (electron and target) is conserved as the electron transfers momentum and thus a small, but measurable, amount of energy to the scattering atom. This energy transfer (the recoil energy) results in an energy loss of the scattered electron. The amount of energy loss of the electron scattering from a particle at rest is given by $E_r = q^2/2M$ (where E_r is the energy loss, q is the magnitude of the momentum transfer \mathbf{q} and M is the mass of the atom). Further, even at 0 K the atoms are vibrating in the lattice. This produces a Doppler broadening of the elastic peak such that the energy loss of an electron scattering from a target with momentum \mathbf{p} is given by:

$$E_r = \frac{q^2}{2M} + \frac{\mathbf{q} \cdot \mathbf{p}}{M} \quad (1)$$

Thus, for high-momentum transfer the elastic peak will split into peaks individual for each of the constituent elements (with atomic mass M) with a peak width which is related to the vibration motion of that nucleus in the lattice.

*Correspondence to: M. R. Went, Atomic and Molecular Physics Laboratories, Research School of Physical Sciences and Engineering, Australian National University, Canberra, ACT 0200, Australia. E-mail: michael.went@anu.edu.au

The intensity of electrons scattered from each constituent element is proportional to the elastic cross-section at the chosen scattering angle which, to a first approximation, can be described by the Rutherford cross-section and is thus proportional to Z^2 , with Z being the atomic number.

Only electrons that have not scattered inelastically will contribute to the elastic peak. The probability (I_l) that an electron has not scattered inelastically decreases with l , the path length inside the material as:

$$I_l = e^{-l/\lambda} \quad (2)$$

where λ is the inelastic mean free path (IMFP).

Thus, for a reflection ERBS experiment of a homogeneous system the elastic signal on average comes from electrons which have a total path length of

$$\frac{\int_0^\infty l e^{-l/\lambda} dl}{\int_0^\infty e^{-l/\lambda} dl} = \frac{\lambda^2}{\lambda} = \lambda \quad (3)$$

In the work presented here, the sample can be rotated around the vertical axis which in turn changes the incident (θ_{in}) and outgoing (θ_{out}) angle that the electron beam makes with the surface normal. In this way, the average signal depth ($\bar{\delta}$) at which the electrons scattered elastically can be varied. Figure 1 shows a schematic representation of the measurement, it follows from this figure that the average signal depth is related to θ_{in} , θ_{out} and the IMFP by

$$\bar{\delta} = \frac{\cos \theta_{\text{in}} \cos \theta_{\text{out}}}{\cos \theta_{\text{in}} + \cos \theta_{\text{out}}} \lambda \quad (4)$$

Assuming a single scattering approach, ie. contributions from multiple elastic scattering are minor, then the count

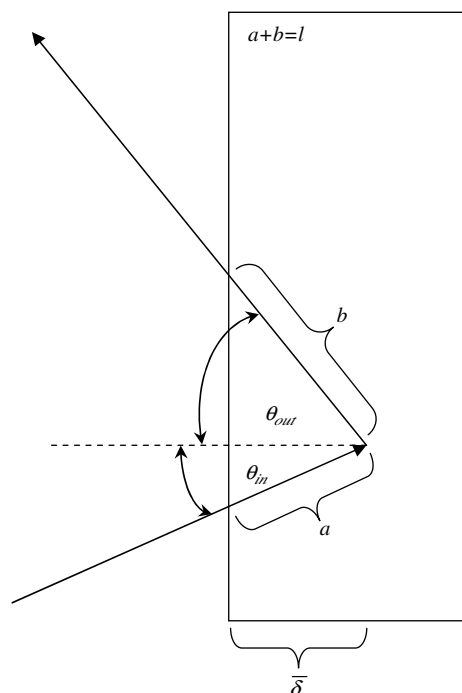


Figure 1. Geometry used to calculate the average signal depth from the incident and outgoing beam angles at the average signal depth $\bar{\delta}$, $a + b = \lambda$.

rate ($I_{\text{Al}}^{\text{hom.}}$) for the elastic peak of a homogeneous Al layer is:

$$\begin{aligned} I_{\text{Al}}^{\text{hom.}} &= C \left(\frac{d\sigma}{d\Omega} \right)_{\text{Al}} N_{\text{Al}} \int_0^{\infty} e^{-l/\lambda_{\text{Al}}} \left(\frac{1}{\cos \theta_{\text{in}}} + \frac{1}{\cos \theta_{\text{out}}} \right) dl \\ &= C \left(\frac{d\sigma}{d\Omega} \right)_{\text{Al}} N_{\text{Al}} \lambda_{\text{Al}} \frac{\cos \theta_{\text{in}} \cos \theta_{\text{out}}}{\cos \theta_{\text{in}} + \cos \theta_{\text{out}}} \end{aligned} \quad (5)$$

With C , a constant, determined by the experimental conditions (beam current, detector opening angle, etc). For an overlayer-substrate system, this becomes slightly more complicated. Consider the special case of an Al_2O_3 overlayer (with thickness a) on aluminium. The substrate contribution is attenuated from the value given by Eqn (5) as electrons scattered elastically from the substrate may scatter inelastically in the overlayer.

$$I_{\text{Al}}^{\text{subst.}} = I_{\text{Al}}^{\text{hom.}} e^{-a/\lambda_{\text{Al}_2\text{O}_3}} \left(\frac{1}{\cos \theta_{\text{in}}} + \frac{1}{\cos \theta_{\text{out}}} \right) \quad (6)$$

The intensity of electrons scattered from oxygen is given by

$$I_{\text{O}} = C \left(\frac{d\sigma}{d\Omega} \right)_{\text{O}} \frac{3}{5} N_{\text{Al}_2\text{O}_3} \int_0^a e^{-l/\lambda_{\text{Al}_2\text{O}_3}} \left(\frac{1}{\cos \theta_{\text{in}}} + \frac{1}{\cos \theta_{\text{out}}} \right) dl \quad (7)$$

For aluminium, the observed intensity is the sum from the contribution of Al in the overlayer and substrate:

$$I_{\text{Al}} = C \left(\frac{d\sigma}{d\Omega} \right)_{\text{Al}} \frac{2}{5} N_{\text{Al}_2\text{O}_3} \int_0^a e^{-l/\lambda_{\text{Al}_2\text{O}_3}} \left(\frac{1}{\cos \theta_{\text{in}}} + \frac{1}{\cos \theta_{\text{out}}} \right) dl + I_{\text{Al}}^{\text{subst.}} \quad (8)$$

In the previous $\left(\frac{d\sigma}{d\Omega} \right)_{\text{O,Al}}$ are the differential elastic scattering cross-sections, $N_{\text{Al,Al}_2\text{O}_3}$ the atomic densities of Al and

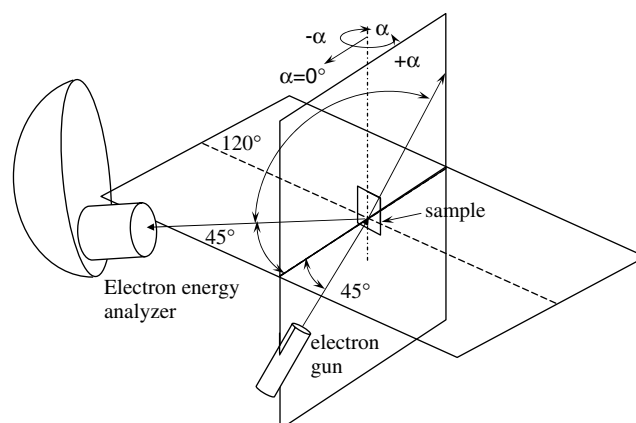


Figure 2. Schematic representation of the experiment. The sample can be rotated around the vertical axis to change the depth sensitivity. If the sample surface normal is in the vertical plane through the gun, $\alpha = 0$. The experiment is in its most bulk sensitive geometry when the sample is rotated by $\approx 20^\circ$ towards the analyzer ($\alpha = -20^\circ$) see Fig. (3).

Al_2O_3 , and $\lambda_{\text{Al,Al}_2\text{O}_3}$ the respective IMFP. The elastic cross-sections and IMFPs are available from relativistic partial wave calculations⁵ and TPP-2M calculations,⁶ respectively.

EXPERIMENT

Figure 2 shows the experimental configuration used for the ERBS measurements. An electron gun (Kimball Physics ELG-2 with BaO filament for reduced energy spread ≈ 300 meV) produces a beam of electrons at 550 eV, the electrons are accelerated by the sample which is held at 39 450 kV. Thus, the 40 keV electrons hit the sample. This energy allows the Xe, Al and O elastic peaks to be separated within our experimental resolution. The choice of such a high energy also allows the sample to be investigated over a significant depth. The electron gun is mounted below the horizontal plane at an angle of 45° . The analyzer is placed such that the scattering angle is 120° . At this angle, the mean recoil energy according to Eqn (1) is then 4.3 eV (O), 2.5 eV (Al) and 0.5 eV (Xe), and under these conditions the calculated differential elastic cross-section is $9.02 \times 10^{-23} \text{ cm}^{-2}/\text{Sr}$ for O, $2.44 \times 10^{-22} \text{ cm}^{-2}/\text{Sr}$ for Al and, $6.33 \times 10^{-21} \text{ cm}^{-2}/\text{Sr}$ for Xe).⁵ For Al and O, the cross-sections increases proportional to Z^2 (as expected for the Rutherford cross-section), but for Xe the increase in cross-section is less than expected from the Rutherford formula. This is due to screening of the nucleus by bound electrons included in the calculations but absent in the Rutherford cross-section. At 40 keV, the IMFP as determined by the TPP-2M formula is 544 Å for Al_2O_3 and 528 Å for Al.⁶

Electrons, which scatter from the sample into the entrance slit of the analyzer, are decelerated to 200 eV and focussed at the entrance of a hemispherical electron-energy analyzer. The scattered electrons are energy dispersed as they pass through the analyzer. Electrons that scatter elastically and with small energy loss (< 40 eV loss) are detected simultaneously by the two-dimensional detector at the exit of the electron-energy analyzer. Electron-energy loss spectra can be obtained

over a wider energy range by scanning the potential of the analyzers. Scanning also corrects for inhomogeneities in the channel plate efficiency. The electron-energy analyzer is mounted in the horizontal plane at 45° to the plane formed by the gun and the vertical direction. The electron-energy analyzer has been described in more detail elsewhere.⁷

Beam currents for these measurements are typically 5 nA. Measurements generally take 1.5 h and consist of a number of scans across the region of interest (elastic peak). With the elastic peak centered on the detector count rates are of the order of 200 Hz. Signal-to-noise ratio is determined from the "dark counts" in the region of negative energy loss and the total counts in the elastic peak and is greater than 300:1.

By rotating the sample around the vertical axis, the angle that the incident and outgoing electrons make with the surface changes, and thus the length over which the electrons, originating from a certain depth, travel is either increased or decreased. This changes the sensitivity of the technique from depth sensitive when the sample normal is toward the analyzer to more surface sensitive when it is rotated away (Fig. (3)).

RESULTS AND DISCUSSION

First, an aluminium foil sample (99.99% purity: metal content only, supplied by Alfa Aesar) was cleaned with ethanol and placed in the vacuum. In the ERBS measurement, the elastic peak showed a small shoulder at the positive energy loss side of the main aluminium peak (Fig. (4)). As the absolute energy scale of our apparatus is unknown within $\approx \pm 0.5$ eV, the peak positions cannot be measured. As such, the main elastic peak is aligned with the expected recoil energy for Al (2.53 eV). The shoulder appears then at an energy that corresponds to the recoil energy for oxygen (4.21 ± 0.03 eV) in good agreement with 4.27 eV as predicted by Eqn (1). For each spectra, the peak areas were determined by nonlinear fitting using two Gaussians, one for each constituent element. Doppler broadening is clearly resolved as the full width at half maximum (FWHM) of the aluminium and oxygen

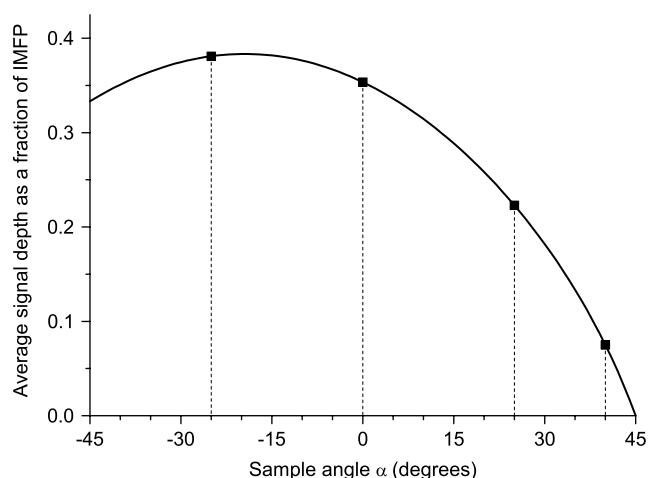


Figure 3. Average signal depth for homogeneous materials as a fraction of the IMFP for accessible sample angles as calculated using Eqn (4). Squares-indicated angles measured in this work.

are 1.0 ± 0.1 and 1.5 ± 0.1 eV respectively, larger than the experimental resolution of ≈ 0.6 eV.

The relative peak areas Fig. (4) obtained from Gaussian fits of the elastic peaks are then compared with values obtained from Eqns (5)–(8). These calculations use the accepted values for the bulk density and stoichiometry of Al_2O_3 . For the $\alpha = 0$ sample orientation, good agreement with the measurement was found for a layer thickness of ≈ 190 Å. This thickness is more than the oxide thickness that grows on clean Al when exposed to atmosphere (referred to as the native oxide). It is presumably caused by a combination of the native oxide layer and oxygen introduced into the surface by the rolling procedure used in forming the foil. This value is in good agreement with an oxide layer produced at $\approx 300^\circ\text{C}$ ⁸ a surface temperature which would likely be attained during cold rolling.

By rotating the sample to the more surface sensitive position and performing the same measurements, one finds that the relative intensity of the O-peak increases, but not as much as calculated based on Eqns (5)–(8). This would be indicative of an inhomogeneous oxide layer covering the surface. At the 40° position, the average signal depth is 0.08 times the IMFP and so the peak-area ratio Al:O should approach $\sigma_{\text{Al}}N_{\text{Al}}/\sigma_{\text{O}}N_{\text{O}} = 1.803$ ($\approx (13^2 \times 2)/(8^2 \times 3) = 1.76$) for a thick oxide film. The measured value is 2.5, which would support the hypothesis that the film is indeed inhomogeneous as the beam would only need to see a small amount of substrate for this to occur. Le *et al.*⁹ investigated the fracturing of the oxide layer in cold rolled aluminium and found that in the cold rolling process, pure aluminium could be extruded through cracks in the oxide layer. This process will increase the amount of aluminium observed on the surface layer, thus the Al:O ratio could approach that measured.

By changing the angle we change the fraction of the Al signal that originates from the substrate. For $\alpha = 0^\circ$, the majority comes from the substrate; for $\alpha = 40^\circ$ the majority comes from the overlayer. As the bonding of Al in Al metal and in Al_2O_3 is different, its vibrational properties (and hence Doppler broadening) are not necessarily the same. However, we do not observe a clear trend in the Al peak width in Fig. 4.

The sample was then cleaned of the oxide layer by Xe sputtering at 3 keV for ≈ 3 h and $2 \mu\text{A}/\text{cm}^2$ current density with the ion beam perpendicular to the sample surface. In this case, the oxygen peak is removed but a surprisingly large additional peak appears at the low energy loss side of the main aluminium peak Fig. (5). Again by aligning the Al peak with the position determined from Eqn (1) this new peak is centered at 0.56 ± 0.02 eV in good agreement with the calculated energy loss for Xe of 0.52 eV. The peak is therefore attributed to Xe which is implanted into the aluminium surface. The large intensity of the peak can be explained by its large elastic scattering cross-section. The width of the Xe peak (FWHM 0.6 ± 0.1 eV) is less than that of either the aluminium or oxygen peaks and is probably determined mainly by the combined energy resolution of analyzer (< 500 meV) and energy spread of the gun (≈ 300 meV). Measurements of Xe-ion deposition at higher energies have found that these implanted ions precipitate to form bubbles

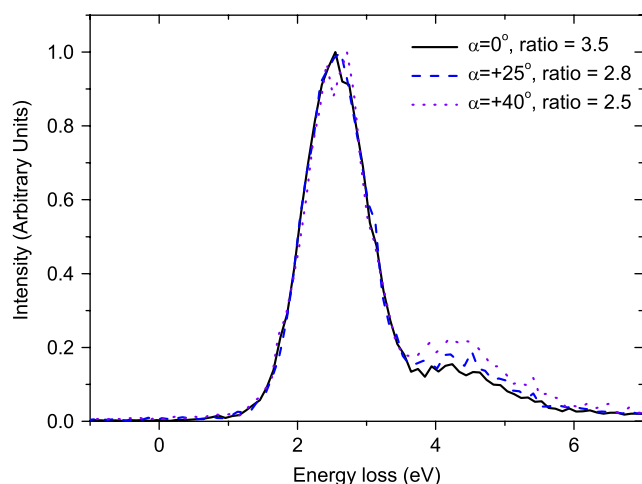


Figure 4. Comparison of the native oxide layer from the raw foil in each of the three measurement geometries. Solid line $\alpha = 0^\circ$, dashed line $\alpha = +25^\circ$ and dotted line $\alpha = +40^\circ$. The ratios of Al- to O-peak area as determined by curve fitting are given in the legend. This figure is available in colour online at www.interscience.wiley.com/journal/sia.

below the surface.^{10–12} Our measurements at this lower energy have found the ions to become similarly trapped in the matrix, however the form of the Xe is unknown. A SRIM¹³ simulation of the sputtering indicates that these ions are implanted at a depth up to $\approx 60 \text{ \AA}$. However, keep in mind that the sputtering process also erodes the surface. By measuring the sample in the 0° , -25° and $+25^\circ$ positions the Xe elastic peak appeared largest in the most surface sensitive measurement. This would suggest that the Xe distribution was centered at a depth smaller than $\bar{\delta}$, the average signal depth. In order to test our understanding aluminium was evaporated on the Xe-cleaned Al film, in three steps: 100, 150

and 150 \AA . Hence, assuming that the Xe-depth distribution after implantation is centered at 60 \AA , after evaporation the Xe 'layer' appears at a total depth of 160, 310 and 460 \AA for the respective aluminium depositions. The thickness of deposited aluminium was calibrated by conventional ion RBS in a separate evaporation on molybdenum.

Table 1 shows the incident and outgoing beam angles for the three sample positions and the average signal depth as a function of the IMFP. These calculations indicate that for an implantation depth of $\approx 0.3 \times$ the IMFP that to a first approximation rotating the sample will have only a small effect on the observed Xe intensity. The energy loss spectra of the 60, 160, and 460 \AA (Xe depth) measurements in each of the three geometries is presented in Fig. (5). These measurements demonstrate three possible cases; where the Xe is above the average signal depth; where the Xe is at the average signal depth and when the Xe is below the average signal depth. It can be clearly seen that in the as implanted film, when Xe is close to the surface, rotating the sample to the surface sensitive position increases the Xe-peak intensity. Alternatively, for Xe that is at a depth of 460 \AA rotating the sample to the bulk sensitive position increases the Xe peak. However, when the Xe is near the average signal depth of the Al, rotating the sample to the three positions causes only small changes in the Xe intensity.

In Fig. (6), we present calculations for the Al-to-Xe ratio for each of the three measurement angles for Xe depths up to 600 \AA for three different values of the IMFP compared to the measurements of the Al:Xe ratio from the depths of 60, 160, 310 and 460 \AA . It can be seen that the average signal depth (where the three lines are closest) changes as the IMFP varies. The measurement is in agreement with the TPP-2M calculation¹⁴ of the IMFP 528 \AA .

Finally, we prepared a clean aluminium surface by evaporating 1500 \AA of Al (99.98%) over an aluminium

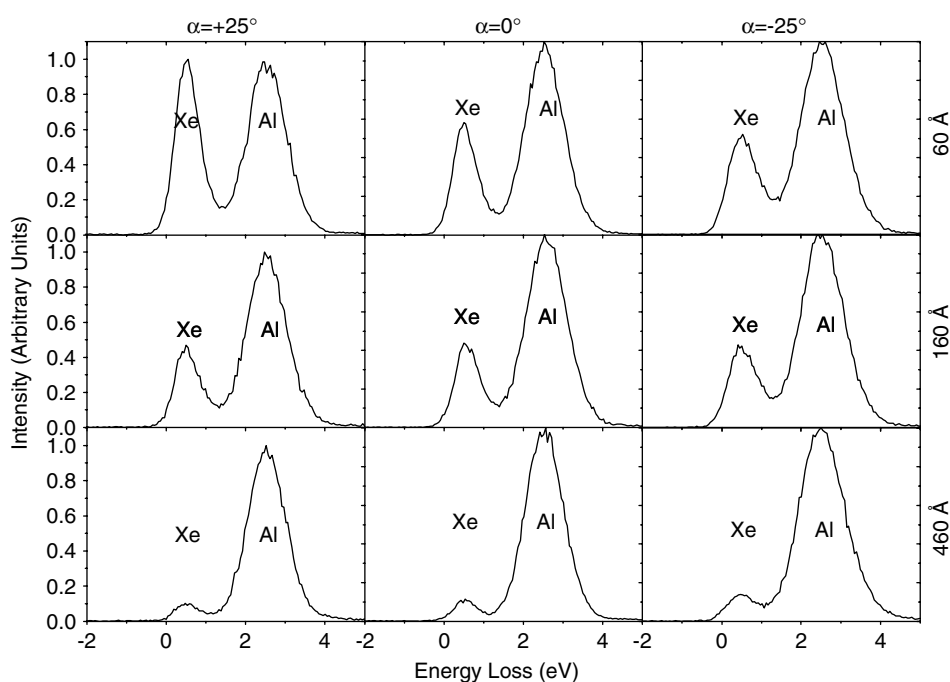


Figure 5. Measurements of the elastic peak for Xe-implanted Al for three Xe depths and the three sample angles.

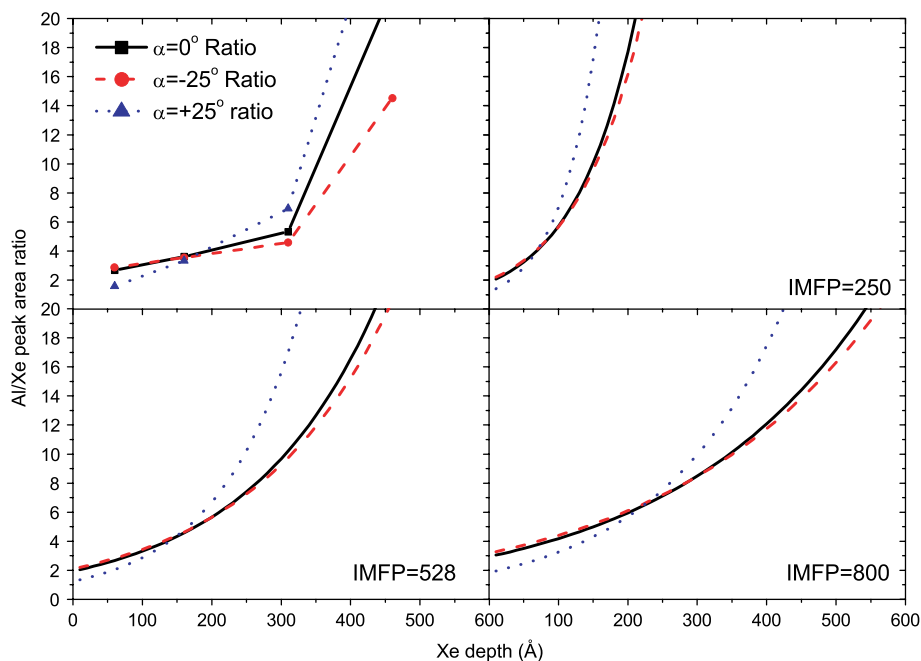


Figure 6. Calculated peak ratios for each of the three geometries for Xe impurities in Aluminium at different depth, compared to the measured peak ratios (top left). Calculations were done assuming different values for the inelastic mean free path, as indicated. Solid line $\alpha = 0^\circ$, dashed line $\alpha = -25^\circ$, dotted line $\alpha = +25^\circ$. This figure is available in colour online at www.interscience.wiley.com/journal/sia.

Table 1. Angular values for each of the three sample positions and the associated average signal depth

Description	Sample angle α ($^\circ$)	Incident angle θ_{in}	outgoing angle θ_{out}	average signal depth $\bar{\delta}$
Bulk sensitive	-25°	50°	20°	0.38λ
Normal	0°	45°	45°	0.35λ
Surface sensitive	$+25^\circ$	50°	70°	0.22λ
Extremely surface sensitive	$+40^\circ$	57°	85°	0.08λ

substrate. The cleanliness was confirmed with ERBS; no sign of oxygen was present in the measurement (Fig. (7)) and the elastic peak consisted of only one component. The sample was then removed from the vacuum and exposed to air at 21°C for approximately 2×10^5 s before being returned to vacuum and measured again with the ERBS technique at the -25° , 0° and $+25^\circ$ orientations. The native oxide layer was determined to be 55 ± 10 Å thick in reasonable agreement with measurements by other groups^{15,16} who determined the native oxide layer to be ≈ 40 Å thick. Figure (7) also shows that the oxygen peak is indeed larger for the rolled film than for the film oxidized in air.

By changing α to 40° , the outgoing electrons become very glancing (85°). Now, even at such large glancing angles, the substrate still contributes (as the oxide overlayer is quite thin) and given the difference in cross-section between Al and O if the beam ‘sees’ only a small amount of substrate it will affect the observed ratio considerably. The Al:O peak-area ratio is found to be 8.7:1 while that calculated from Eqns (5)–(8) (assuming a oxide film thickness of 55 Å) is 2.9:1

in comparison to 1.76:1 (assuming bulk oxide) determined from the simple ratio $\sigma_{Al}N_{Al}/\sigma_{O}N_{O}$. One explanation may be the rough nature of the evaporated film, and the spectrum is mainly due to those surfaces for which the outgoing angle is less than 85° .

SUMMARY AND CONCLUSION

Measurements using the ERBS technique have been used to determine the thickness of the oxide layer caused by cold

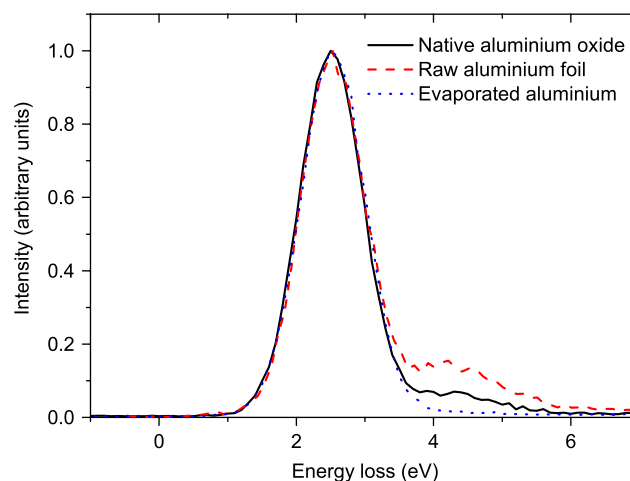


Figure 7. Comparison of ERBS measurements from clean aluminium, the oxide layer from cold rolling and the native oxide layer formed by exposure of clean aluminium to air. All measurements taken with $\alpha = 0^\circ$. Solid line, native aluminium oxide; dashed line, raw aluminium foil; dotted line evaporated aluminium foil. This figure is available in colour online at www.interscience.wiley.com/journal/sia.

rolling. From measurements in a bulk sensitive geometry, we obtain an oxide thickness of ≈ 190 Å, which is good agreement with other measurements of an oxide layer created in air at 300 °C.⁸ At large glancing angles, the Al:O peak-intensity ratio does not approach the ratio calculated for Al₂O₃ which suggests that the oxide film is inhomogeneous.

The oxide layer created by exposing a freshly deposited aluminium layer to air was determined to be 55 ± 10 Å in comparison to a value of ≈ 40 Å as determined by other groups.^{15,16} Measuring at large glancing angles (85° between surface normal and analyzer) again does not lead to the peak-intensity distribution as calculated for an Al₂O₃ compound. In this configuration, we see more Al than expected. This could be explained by the rough nature of the evaporated films. However, there is an alternate explanation for the deviation observed at large glancing angles. A similar problem has been observed before for other stoichiometric compounds² and was then attributed to errors in the calculated cross-sections. The same could be true for the discrepancy seen in the large angle measurement of the cold rolled aluminium foil and oxidized evaporated films.

This technique has also been used to examine ion implantation of Xe into an Al matrix. When the implanted layer is centered at smaller depth than the average signal depth, the signal from the Xe layer can be increased by making the measurement more surface sensitive and vice versa. As the average signal depth is related to the IMFP of electrons in the material, we have found good agreement between our measurement and a TPP-2M calculation of the IMFP of aluminium at 40 keV.

Doppler broadening is clearly resolved for Al and O as their observed width (1.0 ± 0.1 eV and 1.5 ± 0.1 eV respectively) is larger than the width of the Xe peak (0.6 ± 0.1 eV). The FWHM of the peaks is clearly related to its mass (as expected from Eqn (1)), with lighter elements exhibiting a larger Doppler broadening.

In this work, a strong dependence on Z for detection in an ERBS spectrum has been shown. For heavy impurities in a light substrate, the ERBS technique does very well and only a small amount of the heavy element (Xe in this case) is required for a strong elastic peak to be observed. In cases where light elements are in the presence of heavy

elements (oxygen into aluminium), the large difference in cross-section ($\propto Z^2$) means that even for cases where the light element constitutes the majority, as in the case of Al₂O₃, their contribution to the elastic peak is small. Thus small amounts of a light element will be difficult to detect in a heavy element matrix. In the case where the two elements are of similar mass, the Doppler broadening of the individual peaks means that their peaks can not be resolved.

In general, ERBS is an electron spectroscopy with a rather unique set of characteristics. We think that it has the potential to be developed into a quantitative surface analysis technique, especially for study of materials on a somewhat larger depth-scale than can be studied by conventional electron spectroscopy using energies of ≈ 1 keV and less.

Acknowledgements

This research was made possible by a grant of the Australian Research Council. The Authors would like to acknowledge the assistance of R.G. Elliman in performing the convention ion RBS calibration.

REFERENCES

1. Went M, Vos M, Elliman R. *J. Electron Spectrosc. Relat. Phenom.* 2007; **156–158**: 387.
2. Went M, Vos M. *Appl. Phys. Lett.* 2007; **90**(2): 072104.
3. Vos M, Went M. *J. Electron Spectrosc. Relat. Phenom.* 2007; **155**(1–3): 35.
4. Went M, Vos M. *Surf. Sci.* 2006; **600**: 2070.
5. Salvat F, Jablonski A, Powell C. *Comput. Phys. Commun.* 2005; **165**: 157.
6. Tanuma S, Powell C, Penn D. *Surf. Interface Anal.* 1993; **21**: 165.
7. Vos M, Cornish GP, Weigold E. *Rev. Sci. Instrum.* 2000; **71**: 3831.
8. Smeltzer WW. *Journal of the Electrochemical Society* 1956; **103**(4): 209.
9. Le H, Sutcliffe M, Wang P, Burnstein G. *Acta Mater.* 2004; **52**: 911.
10. Potter D, Rossouw C. *J. Nucl. Mater.* 1989; **161**: 124.
11. Ishikawa N, Awaji M, Furuya K, Birtcher R, Allen C. *Nucl. Instrum. Methods Phys. Res., Sect. B* 1997; **127/128**: 123.
12. vom Felde A, Fink J, Müller-Heinzerling T, Pflüger J, Scheerer B, Linker G. *Phys. Rev. Lett.* 1984; **53**(9): 922.
13. Ziegler J, Biersack J, Littmark U. *The Stopping and Range of Ions in Solids*. Pergamon Press: New York, 1985.
14. Tanuma S, Powell C, Penn D. *Surf. Interface Anal.* 1993; **20**: 77.
15. Feliu S Jr, Bartolomé M. *Surf. Interface Anal.* 2007; **39**: 304.
16. Cabrera N, Mott N. *Rep. Prog. Phys.* 1949; **12**: 163.